Improving the Accuracy of Size/Micro Strain Estimation by First Principles Monte Carlo Raytraced Fundamental Parameter Profiles

J.Bergmann[1], R.Kleeberg[2]

1: Ludwig-Renn-Allee 14, D-01217 Dresden, Germany
2: University of Mining and Technology, Institute of Mineralogy, Brennhausgasse 14, D-09596 Freiberg, Germany

ABSTRACT

In the Monte Carlo raytraced FPA (fundamental parameter approach), the true slit dimensions, their distances and other geometric features are used as input parameters to follow the beam paths inside the diffractometer. In a first trial, this model failed in describing the profile standard SRM 660 (NIST standard reference material) as measured using different devices and X-ray tubes. The reason could be addressed to the real emission profile of the commercial X-ray tubes: 5%...30% of the X-rays do not originate from a proper rectangular X-ray focus. The intensity coming from both sides of the focus was called "tube-tails". In a second step, the raytraced FPA has been corrected by measuring the focus intensity distribution and including this measurement in the Monte Carlo raytracing algorithm. Now, SRM 660 gave a main micro grain diameter (size) of 725(8) nm and a micro stress of 0.000075(4). For the new SRM 660a a zero micro strain and 1456(20) nm size have been determined. However, the Rietveld plot of SRM 660a deviated significantly from a clean random difference curve. Additionally, a dynamic extinction/absorption correction to the diffraction profile was introduced. Now, a micro strain of 0.000058(2) and an insignificant large size $> 2\mu$m was calculated for SRM 660a. SRM 660 did not show a dynamic effect. SRM 660 has a clear micro size structure. SRM 660a seems to have a size value near to the macroscopic grain size.

INTRODUCTION

Size/micro strain estimation by profile refinement demands for an accurate ideal peak shape model. Traditionally, simple analytic profile functions have been used (see e.g. [1]). However, they fail to describe the asymmetry of real XRPD lines, which is caused by the geometry of the diffractometer. More sophisticated methods use "learnt profiles". Here, the summed contributions of the wavelength distribution and the geometric aberrations are determined from measured profiles at an ideal sample. These ideal profiles are represented either by numerical fitting [2], or by Fourier coefficients [3]. This method enables the analysis of phase-specific real structure broadening models. Only the broadening caused by the diffraction process (real structure etc.) must be refined. The disadvantage is the restriction of the 2Θ range by the line positions of the standard.

The so called "fundamental parameter approach" (FPA) methods use a folding of separate wavelength distribution functions, geometric profiles and diffraction broadening models. A description for the neutron diffraction leads to the well discussed U, V, W parameters [4]. Problems during the simultaneous refinement of U, V, W have been well discussed elsewhere [1]. The XRPD geometric conditions are more complicated. Therefore, one needs more fundamental parameters then U, V, W. For example, Kogan & Kupriyanov [5], as well as Cheary & Coelho [6], [7], gave a description depending on some more realistic parameters such as

- focus width;
- primary plus secondary axial divergence angles;
- detection slit width;
- sample's penetration depth;
- equatorial divergence angle.

Analogously to the problems with U, V, W, convergence problems may occur while refining multiples of the XRPD fundamental parameters. Cheary & Coelho [7], for example, have only refined one parameter themselves.

But the XRPD profile description is much more complicated. Even a dozen parameters are not

enough to describe the real ray paths. Here is an example:

The two parameters, primary and secondary divergence, are a combination of the axial focus dimension, several primary axial slits, the axial sample dimension, secondary axial dimensions (e.g. axial monochromator dimension), the axial detection slit dimension, plus others. In the case of a finite round sample, the axial divergence depends on the equatorial divergency angle.

Therefore, the simple fundamental parameter profiles [7] must be somewhat "refined" for a good fit to the experimental data. Why not use a much more complicated fundamental parameter description? The result can no longer be represented in a closed expression. Half a dozen nested integrals must be solved numerically. This requires for large futuristic supercomputers, if refined. On the other hand, such deeply nested integrals may be solved by Monte Carlo integration.

PRINCIPLES OF THE FUNDAMENTAL PARAMETER PROFILES

Basically, each line in a given diffraction pattern may be described by a three-fold convolution

$$I = \mathbf{\Lambda} * \mathbf{G} * \mathbf{P} \quad (1)$$

where

$$\mathbf{\Lambda} = \text{spectral distribution of the characteristic } K_\alpha \text{ doublet of the X-rays} \quad (2)$$

$$\mathbf{G} = \text{geometric response function of the diffractometer} \quad (3)$$

$$\mathbf{P} = \text{ideal diffraction function of the sample} \quad (4)$$

In doing so, we assume that the geometric response function does not depend on the wavelength of the X-rays. This is valid for all conventional slit setups, including those with a secondary monochromator behind the detection slit. It is invalid for primary monochromators. From the author's experience, (1) holds for modern reflection optics. It also holds for PSD counting devices.

The best values for $\mathbf{\Lambda}$ are given in Hölzer *et al.* [8]. They yield parametrizations of $\mathbf{\Lambda}$ as sums of Lorentzians, being suggested by the theory of spectral emission.

The convolution (1) demands efficient numeric treatment by the implementing programs. In general, convolutions are handled by (fast) Fourier transforming any parts and re-transforming the result. This method is used by Kogan & Kupriyanov [5], as well as by Cheary & Coelho [6], [7]. Here, another method is used for an efficient numeric handling of the threefold convolution procedure.

THE RAYTRACING METHOD FOR THE CONSTRUCTION OF G

First Principles Raytracing

From now on, the conventional Bragg-Brentano geometry is assumed. Equivalent algorithms have been developed for transmission (planar) and capillary Debye Scherrer geometries.

Fig. 1 shows the simplest case of the geometry description. The following parameters *must* be supported for an exact profile calculation:

- axial and equatorial optical focus dimension;
- position plus width of the primary equatorial divergence slit, may depend on 2Θ;
- take-off angle of the primary axial soller slit *or* height plus position of a primary axial divergence slit;
- length plus axial dimension, *or* diameter of the sample (while raytracing, the penetration depth of the sample will be neglected);
- equatorial detection slit dimension, may depend on 2Θ
- axial dimension of detection slit, *or* axial dimension plus position of the monochromator.

Additional features may be described, for example:

- axial shift plus torsion around a radial axis of the focus;
- secondary anti-scattering slit, may depend on 2Θ;
- Ω tilt of the sample;
- secondary soller slit.

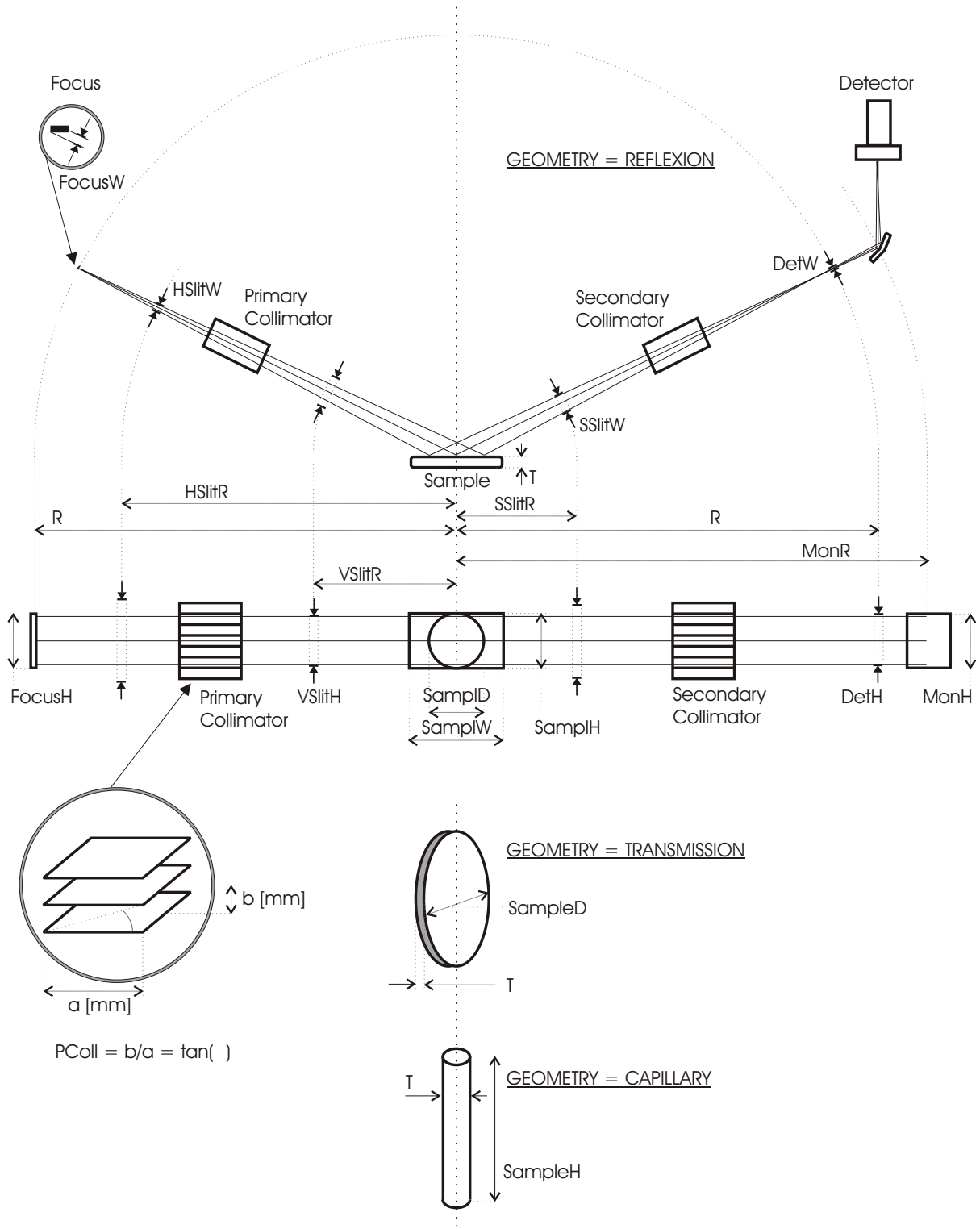

Figure 1: The simplest geometry description as used by the raytracing algorithm, further details may be added.

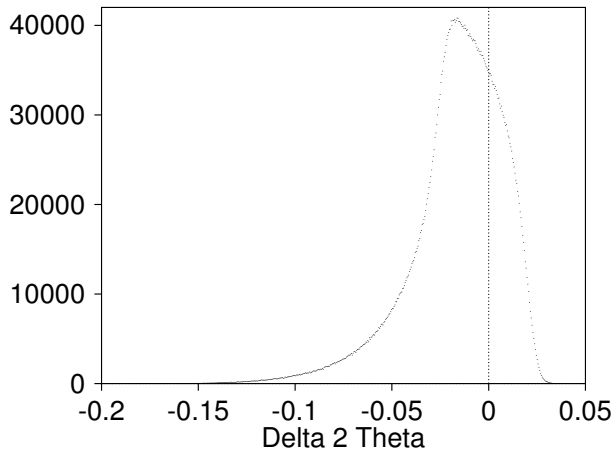

Figure 2: Raw data (event counts per channel) for an exemplary diffractometer set-up.

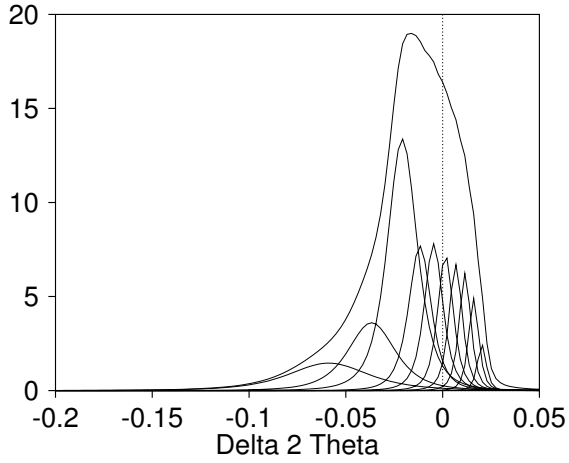

Figure 3: Data from fig. 2 as normalized and fitted by a sum of 10 squared Lorentzians.

The profile is raytraced at a fixed set of angles Θ_0. For each Θ_0, a large number of random events (counts) is computed as follows: A random starting position is chosen inside the optical tube focus. Further random numbers are:

- the equatorial position inside the equatorial divergence slit;
- the axial position inside the axial divergence slit, *or* the axial angle inside the primary soller slit. In the event that the ray path does not reach the sample area, the event will be marked as "failed";
- the equatorial position in the detection slit. In the event of the ray being screened by the anti-scattering slit, the event will be marked as "failed";
- the axial position inside the detection slit, *or* on the monochromator;
- *or* the axial angle in the secondary soller slit. In this case, the ray may axially fail the detection slit, or the monochromator and is therefore marked.

For each event, the real Bragg angle Θ, which will occur between the real primary and the secondary ray path at the specimen's surface, is computed. This gives a difference $\Delta\Theta = \Theta - \Theta_0$. The range of possible $\Delta\Theta$ values is covered by a narrow grid (equivalent to the behavior of a multi-channel analyzer as known from PSDs). After having reached a given number of events in the maximum channel, this random process is stopped. As a result, we have a representation of the geometric profile as a collection of noisy points, see fig. 2.

An equivalent method is used in the fields of multimedia while constructing "imaginary worlds" and the rendering programs there are called "raytracing programs". Following this equivalence, we call the method "raytracing fundamental parameter profiles".

For purposes of further numeric handling (that means folding procedures with $\mathbf{\Lambda}$ and $\mathbf{G}$), this data set must be converted into a suitable representation. The traditional way is a Fourier representation. Here, another representation is chosen: The noisy points are fitted by a growing number of squared Lorentzian functions, until a given precision is reached. This method has two advantages:

1. $\mathbf{\Lambda}$ as given in [8] is parametrized as sums of Lorentzians. $\mathbf{P}$ may be described by sums of Lorentzians (for simplification), this gives an effective and low-parametric representation of the sample's diffraction function. Each finite sum of Lorentzians folds simply by each other finite sum of Lorentzians. The result is a finite sum of Lorentzians, too.
2. Fitting the noisy point-by-point representation of $\mathbf{G}$ by squared Lorentzians is an effective way of smoothing this curve.

For example, Fig. 3 gives the representation of the random points as a sum of squared Lorentzians.

Doing so gives a set of geometric profiles at finite angles (say, a dozen angles Θ_0). Following this, these geometric lines are interpolated for each angle by computing weighted sums of the neighbouring lines. While doing so, the interpolated lines may be corrected for the sample's penetration depth and the finite sample thickness. The weighted sums are fitted by sums of squared Lorentzians, again.

This two-step algorithm was chosen due to the computing time. Step 1 (raytracing) needs half an hour for a dozen angles, step 2 needs five minutes for hundreds of angles. Carrying step one for hundreds of angles would take a whole day to compute.

Trying these First Principles Raytraced Profiles

This raytracing algorithm was checked while measuring the remaining size/strain values of LaB_6 (NIST reference material SRM 660). For the size/strain model, see [9]. We have used two different diffractometers with different slit set-ups, see table 1.

To be sure, three different X-ray tubes from different manufacturers were used: Siemens (the old glass type, manufactured at the Rudolstadt factory), AEG and Philips. As one may observe from the upper half of table 2, the results do not lie within their tolerances. The raytraced fundamental parameter profiles have to be further improved.

Improving Raytracing by Tube Tails Correction

Obviously, the differences occur while changing the X-ray tubes. For a deeper insight, the focus of the X-ray tube was examined as follows: A lead foil with a small hole ($< 50\mu$m) was placed on the axis of the diffractometer. Some damping material was additionally placed into the X-ray path. We used a very narrow detection slit of 50μm. So we measured an intensity distribution as shown in fig. 4.

Obviously, a relevant part (5%...30%) of the X-rays is not produced from a proper rectangular line focus shape, but from supplementary tails on both sides of the optical focus. This effect depends on the type, the manufacturer, the voltage/current and the life stage of the tube and was called "Tube Tails".

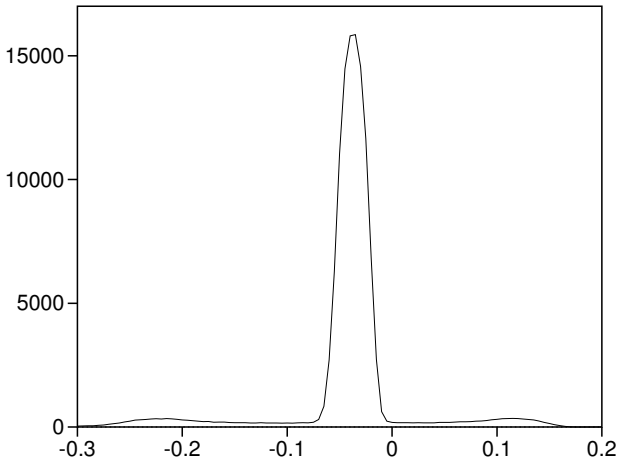

Figure 4: Intensity distribution around the focus as measured for an older AEG fine focus tube. A lead foil with a hole less than 50μm hole was placed at the sample position and was used for the reproduction of the tube focus onto the receiving slit.

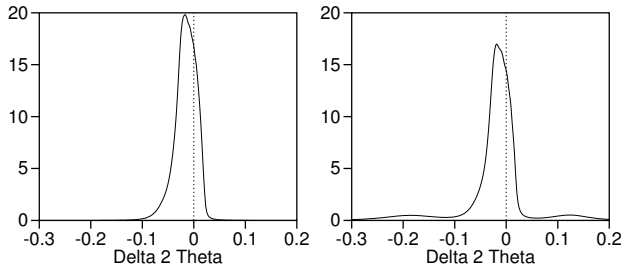

Figure 5: Raytraced geometric part **G** at 2Θ=50 deg according to the XRD3000TT set-up given in table 1. Left: without tube tails correction, right: with tube tails correction.

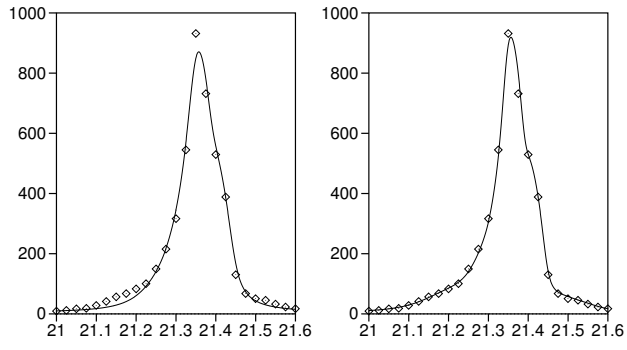

Figure 6: Rietveld plots for the (100) line of the SRM 660 standard. Left: without tube tails correction (R_{wp}=16.02%), right: with tube tails correction (R_{wp}=12.55%). R_{exp} was 10.51%.

Table 1: Exemplary geometric set-ups (complete inputs in the raytracing algorithm).

Goniometer type	XRD3000TT	URD6
goniometer circle radius	250mm	220mm
optical focus dimensions: axial equatorial	 12mm plus 1mm shift 0.04mm	 12mm 0.04mm
primary Soller slits (lamellar distance/length)	0.5/25	0.5/20
axial slit	8mm at radius 128mm (for diminishing the influence of the axial focus shift)	—
equatorial divergence slit	1.5mm at radius 98mm, *or* variable slit, irradiated sample length 10mm	1mm at radius 119mm
sample dimensions	$25\times25mm^2$ (quadratic)	25mm diameter (round)
receiving slit: equatorial dimension (does not terminate ray paths axially)	 0.2mm	 0.25mm
secondary monochromator: distance behind receiving slit axial dimension (terminates ray paths axially)	 52mm 15mm	 59mm 15mm

The simulation of the tube tails was introduced into the raytracing algorithm. Corresponding to a measurement as given in figure 4, a determined part of the random ray paths originates outside the proper rectangular line focus. Fig. 5 compares both, the raytraced geometric parts **G** with and without tube tails correction.

Table 2 illustrates the success of the tube tails correction. Tube tails are the strongest fault of classical fundamental parameter profile description. The measurements clearly show the imperfectness of line profile standards. The total error of the approach is much less compared to line standard imperfectness.

The Rietveld plots, as well as the R_{wp} values, also demonstrate the success of the tube tails correction (see figure 6).

Reference Material NIST SRM 660a

In September 2000, the new NIST peak position and peak profile reference material SRM 660a became available. It was certified for homogeneity and lattice parameter [10]. Efforts were undertaken to achieve a minimum line broadening due to size/strain and optimum grain statistics. A domain size of 2.0 μm and a microstrain below detection limit were given as non-certified values. Electron-microscopic crystallite sizes were observed from 2 to 5 μm [10]. Due to the applied sieving procedure, the aggregated grains were restricted in size to 15 μm. This was confirmed by LASER diffraction. Therefore (and due to the excellent purity), the reference material SRM 660a is expected to be suitable for profile extraction. The following questions have to be answered:

- Is a more detailed real structure characterisation possible? In particular, where does the contradiction between observed X-ray and LASER beam size values come from?
- Does the grain statistic of SRM 660a enable the extraction of the device profiles from narrow lines (multilayer-mirrors etc.)?

Characterisation of SRM 660a

The data was acquired using an XRD 3000 TT diffractometer (Seifert, Ahrensburg). The goniometer radius was 250 mm. The diffractometer was equipped with a Cu long fine focus tube and a secondary graphite monochromator. A detection slit width of 0.2 mm was chosen and primary soller slits and a fixed divergence slit were used. 11001 data points were collected from 15 to 125 deg 2Θ

Table 2: Comparison of size/strain values of SRM 660 as obtained using three different tube types and deconvoluted, with and without tube tails correction

Diffractometer	XRD 3000	XRD 3000	XRD 3000	URD6
Tube manufacturer	AEG	Rudolstadt	Rudolstadt	Philips
Tube anode	Cu	Cu	Cu	Co
Equatorial divergence slit	fixed	fixed	variable	fixed
without tube tails correction				
size/nm	308(4)	468(6)	474(5)	610(10)
micro strain $\times 10^6$	0	0	0	0
with tube tails correction				
size/nm	884(31)	793(23)	824(21)	944(34)
micro strain $\times 10^6$	115(8)	105(8)	113(6)	96(10)
Cheary & Coelho (1998)				
size:	$1.3(7)\mu$m			

at a step size of 1/100 deg and a constant measuring time of 10 s per step. Refinement was carried out using the Rietveld program BGMN. Its fundamental parameters profiles were corrected for the measured tube tails. A mean crystallite size of 1.456(20) μm and no micro strain were obtained. This corresponds to the results given in [10].

However, the SEM observations [10] and the preparation proccess by grinding and annealing of a hard and brittle material indicate a domain size close to the grain size, as well as some minor micro strain due to surface tension. A more sophisticated profile model may consider the dynamic effect of extinction [11], [12]. The latter is not described by the geometric (kinematic) theory of diffraction, which is commonly used in the fields of powder diffraction. Therefore, a very simple extinction correction to the line width was introduced.

Extinction corrected line profiles

The extinction length Λ_0 [11] is commonly used for the discussion of dynamic effects. For LaB_6 (SRM 660a), it is in the order of 1 μm. Following the SEM results [10], one must use the dynamic scattering theory. Additionally, LaB_6 is an highly absorbing specimen. In contrastiction to Si-powder (where one may use the simple dynamic theory without absorption), one must use the dynamic theory for absorbing specimens.

Due to the high absorption, the Bragg case (reflection) is used. Transmission will occur with significantly reduced intensity. We start using the ideal Darwin case (non-zero, but negligible absorption). In order to use the results in the BGMN Rietveld program, the complicated diffraction patterns [12] are approximated by a Lorentzian function of equal total intensity and equal asymptotic behaviour for large angular misfits $|y|$ (equal long-range peak tails). In an angular scale, as used in the dynamic diffraction theory, the Lorentzian width parameter b_1 results as

$$b_1 = \frac{3\pi}{32}\delta \tag{5}$$

$$= \frac{3\pi}{32}\frac{\lambda\,|\gamma_h|}{\Lambda_0 \sin 2\Theta} \tag{6}$$

$$= \frac{3\pi}{32}\sqrt{|\gamma|}\frac{\lambda^2 RC\sqrt{F_h F_{\bar{h}}}}{\sin 2\Theta\,\pi V} \tag{7}$$

with

$$R = \frac{e^2}{mc^2} \tag{8}$$

one electron diffraction strength

λ : X-ray wavelength

F_h : structure factor of the observed reflection

$F_{\bar{h}}$: structure factor of its inverse

$$\sqrt{|\gamma|} = \sqrt{\left|\frac{\gamma_h}{\gamma_0}\right|} \tag{9}$$

$$\gamma_0 = \cos(\vec{n}, \vec{e}_0) \tag{10}$$

$$\gamma_h = \cos(\vec{n}, \vec{e}_h) \tag{11}$$

C : dynamic polarization factor.

$\vec{e}_0$ and $\vec{e}_h$ are the directions of the primary and the diffracted beam respectively. $\vec{n}$ is normal to the crystal surface. Due to the non-planar grain size, $\sqrt{|\gamma|}$ must be discussed in detail later.

Now the absorption is introduced. Following [12], absorption mainly influences the central part (maxima) of the diffraction patterns. The asymptotic behaviour for $|y| \to \infty$ remains unchanged. [12] uses the value

$$g = \frac{\frac{1-\gamma}{2}\psi_0''}{C\,|\psi_h'|\,\sqrt{|\gamma|}} \quad (12)$$

$$= \frac{\psi_0''}{2C\,|\psi_h'|}\left(\sqrt{|\gamma|}+\frac{1}{\sqrt{|\gamma|}}\right) \quad (13)$$

($\gamma < 0$ in the Bragg case)

with

$$\psi_0'' = -\frac{\lambda\mu_0}{2\pi} \quad \text{absorption} \quad (14)$$

$$\psi_h' = -\frac{R\lambda^2 F_h}{\pi V} \quad . \quad (15)$$

Numerical trials (numerical integration of the angular dependencies as given by Zachariasen [12]) gives

$$I_{\text{integral}} \sim \frac{e^{\pi|g|}-1}{\pi\,|g|\,e^{\pi|g|}} \quad (16)$$

as an approximation for the integrated intensity behaviour for all values $|g| = 0\ldots\infty$. The relative error is about 1%. As a result, the width of the Lorentzian approximation must be enlarged by the reciprocal of this value.

Now we introduce the diffraction length scale as used by BGMN and in size/micro strain estimation. As a result, we obtain the total width parameter b_1 for an approximated Lorentzian

$$b_{1,\text{dynamic}} = \frac{3\pi}{32}\sqrt{|\gamma|}\frac{2\cos\Theta}{\lambda}\frac{\lambda^2 RC\sqrt{F_h F_{\bar{h}}}}{\sin 2\Theta\,\pi V} \cdot \frac{\pi\,|g|\,e^{\pi|g|}}{e^{\pi|g|}-1} \quad (17)$$

$$= \frac{3\pi}{32}\sqrt{|\gamma|}\frac{\lambda RC\sqrt{F_h F_{\bar{h}}}}{\sin\Theta\,\pi V} \cdot \frac{\pi\,|g|\,e^{\pi|g|}}{e^{\pi|g|}-1} \quad (18)$$

$$|g| = \frac{\mu_0 V}{4CR\lambda\,|F_h|}\left(\sqrt{|\gamma|}+\frac{1}{\sqrt{|\gamma|}}\right) \quad (19)$$

for purely dynamic diffraction.

Following the purely geometric scattering theory, spheric grains with mean diameter $\bar{d}$ (for distribution see [9]) gives a Lorentzian width parameter

$$b_{1,\text{geometric}} = \frac{4}{3\pi\bar{d}} \quad (20)$$

in the diffraction length scale [9].

However, the diffraction of SRM 660a follows neither a purely dynamic nor a purely geometric theory. According to the discussion of absorption, a total Lorentzian width parameter

$$B_1 = \frac{b_{1,\text{dynamic}}}{\tanh\left(\frac{b_{1,\text{dynamic}}}{b_{1,\text{geometric}}}\right)} \quad (21)$$

is assumed using the intensity reduction formula for the thin Bragg case [12]. By following [12], this gives

$$B_1 = \begin{cases} b_{1,\text{dynamic}} & \text{for } \frac{b_{1,\text{dynamic}}}{b_{1,\text{geometric}}} > 1.8 \\ b_{1,\text{geometric}} & \text{for } \frac{b_{1,\text{dynamic}}}{b_{1,\text{geometric}}} < 0.4 \end{cases} \quad . \quad (22)$$

The factor $\sqrt{|\gamma|}$ must now be discussed for the powder diffraction case. In particular, it diverges if γ_0 becomes zero (grazing incidence onto grain surface). The mean influence of this yet unknown value is introduced as a free parameter γ_{mean} as follows:

$$\overline{\sqrt{|\gamma|}} = \sqrt{\gamma_{\text{mean}}} \quad . \quad (23)$$

For reasons of symmetry, equally statistical distribution is assumed for $|\gamma_0|$ and $|\gamma_h|$. Subsequently, $\frac{1}{\sqrt{|\gamma|}}$ is distributed equally to $\sqrt{|\gamma|}$. It follows that

$$\overline{\sqrt{|\gamma|}+\frac{1}{\sqrt{|\gamma|}}} = 2\sqrt{\gamma_{\text{mean}}} \quad , \quad (24)$$

as used in (19).

Extinction corrected size/micro strain values

This correction reduces R_{wp} from 7.90% to 7.64%. The Durbin-Watson value increases from 1.40 to 1.48 (see Tab. 3 and Fig. 7). $\sqrt{\gamma_{\text{mean}}}$ refines to 2.72(3). The size value becomes insignificantly large. Following (22), this means

$$b_{1,\text{geometric}} < \frac{\sqrt{\gamma_{\text{mean}}}}{1.8}\frac{3\pi}{32}\frac{\lambda RC\sqrt{F_h F_{\bar{h}}}}{\sin\Theta\,\pi V} \cdot \frac{\pi\,|g|\,e^{\pi|g|}}{e^{\pi|g|}-1} \quad , \quad (25)$$

which means $b_{1,\text{geometric}} < 0.2/\mu\text{m}$ or $\bar{d} > 2\mu\text{m}$ for a typical LaB_6-reflection. In accordance with the expectations made above, a micro strain of 0.00583(19)% was calculated. A re-measurement and re-evaluation of the older reference material

Table 3: Results of the size/strain analysis of SRM 660a.

extinction correction	no	yes
R_{wp}	7.90%	7.64%
Durbin-Watson	1.40	1.48
size/μm	1.456(20)	>2
micro strain	0	0.00583(19)%

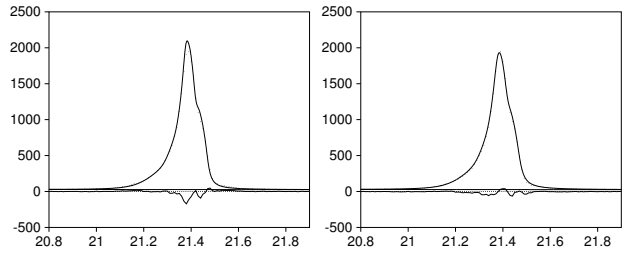

Figure 7: Rietveld difference plots for the 100 lines of SRM 660a. Left without, right with extinction correction.

SRM 660 under equivalent conditions yields the value 0.00890(40)%. As a difference, SRM 660 scatters purely geometricly at a size value of 701(13) nm and no dynamic effect was detectable ($\sqrt{\gamma_{\text{mean}}}$ refines to zero).

CONCLUSION

Raytraced fundamental parameter profiles improve the accuracy of laboratory XRPD size/micro strain estimations. Programs for the construction of these profiles and a Rietveld program for using them were developed. Using these programs, one can obtain more precise size/micro strain values without the need for more precise measurements, or for smaller slits etc. (resulting in higher natural resolution, but otherwise in less intensity plus worse grain statistics). In addition to this, one may make decisions about the truth/falseness of model assumptions, which were impossible using traditional techniques.

References

[1] Young, R.A. and Wiles, D.B., Profile Shape Function in Rietveld Refinements, *J. Appl. Cryst.*, **15**, 430–438, 1982.

[2] Hepp, A., and Baerlocher, C., Learned Peak Shape Functions for Powder Diffraction Data, *Aust. J. Phys.*, **41**, 229–236, 1988.

[3] Le Bail, A., The Rietveld Method Using an Experimental Profile Convoluted by Adjustable Analytical Functions, *Acta Cryst.*, **A40**, Suppl. C369, 1984.

[4] Cagliotti, G., Pauletti, A., and Ricci, F.P., Choice of collimators for a crystal spectrometer for neutron diffraction, *Nucl. Instrum. and Meth.*, **3**, 223–226, 1958.

[5] Kogan, V.A. and Kupriyanov, M.F., X-ray Powder Diffraction Line Profiles by Fourier Synthesis, *J. Appl. Cryst.*, **25**, 16–25, 1991.

[6] Cheary, R.W. and Coelho, A., A Fundamental Parameters Approach to X-ray Line-Profile Fitting, *J. Appl. Cryst.*, **25**, 109–121, 1992.

[7] Cheary, R.W. and Coelho, A.A., Axial Divergence in a Conventional X-ray Powder Diffractometer. II. Realization and Evaluation in a Fundamental-Parameter Profile Fitting Procedure, *J. Appl. Cryst.*, **31**, 851–861, 1998.

[8] Hölzer, G., Fritsch, M., Deutsch, M., Härtwig, J., and Förster, E., K$\alpha_{1,2}$ and K$\beta_{1,3}$ X-ray emission lines of the 3d transition metals, *Phys. Rev.*, **56**, 4554–4568, 1997.

[9] Bergmann, J., Kleeberg, R., Haase, A. and Breidenstein, B., Advanced fundamental parameters model for improved profile analysis, *Mat. Sci. Forum*, **347-349**, 303–308, 2000.

[10] Cline, J.P., Deslattes, R.D., Staudenmann, J.-L., Kessler, E.G., Hudson, L.T., Henins, A., and Cheary, R.W., Certificate Standart Reference Material 660a: Lanthanum Hexaboride Powder, Line Position and Line Shape Standard for Powder Diffraction, NIST, Gaithersburg, 2000.

[11] Authier, A., Dynamical theory of X-ray diffraction, in Int. Tables for Crystallography, U. Shmueli, Ed., Vol. B, pp. 464–480 Kluwer Academic Publishers, Dortrecht, 1996.

[12] Zachariasen, W.H., Theory of X-ray Diffraction in Crystals, Reprint ed., Dover Publ., New York, 1994.